Supplementary Information

Supported pulmonary surfactant bilayers on silica nanoparticles: Formulation, stability and impact on lung epithelial cells

F. Mousseau[1*], C. Puisney[2], S. Mornet[3], R. Le Borgne[4], A. Vacher[5], M. Airiau[5], A. Baeza[2] and J.-F. Berret[1*]

Outline

Supporting Information Figure S1 – Determination of Curosurf® vesicle membrane thickness

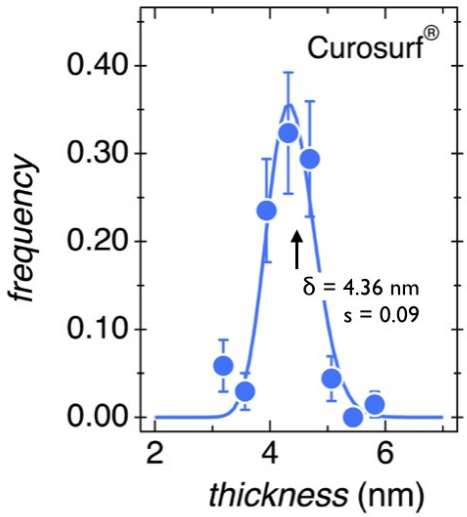

Figure S1: *Distribution of Curosurf® membrane thickness obtained by cryo-TEM. The average value is δ = 4.36 nm. The distribution was determined on n = 68 measurements.*

Supporting Information S2 – Additional cryo-TEM images of Curosurf® vesicles

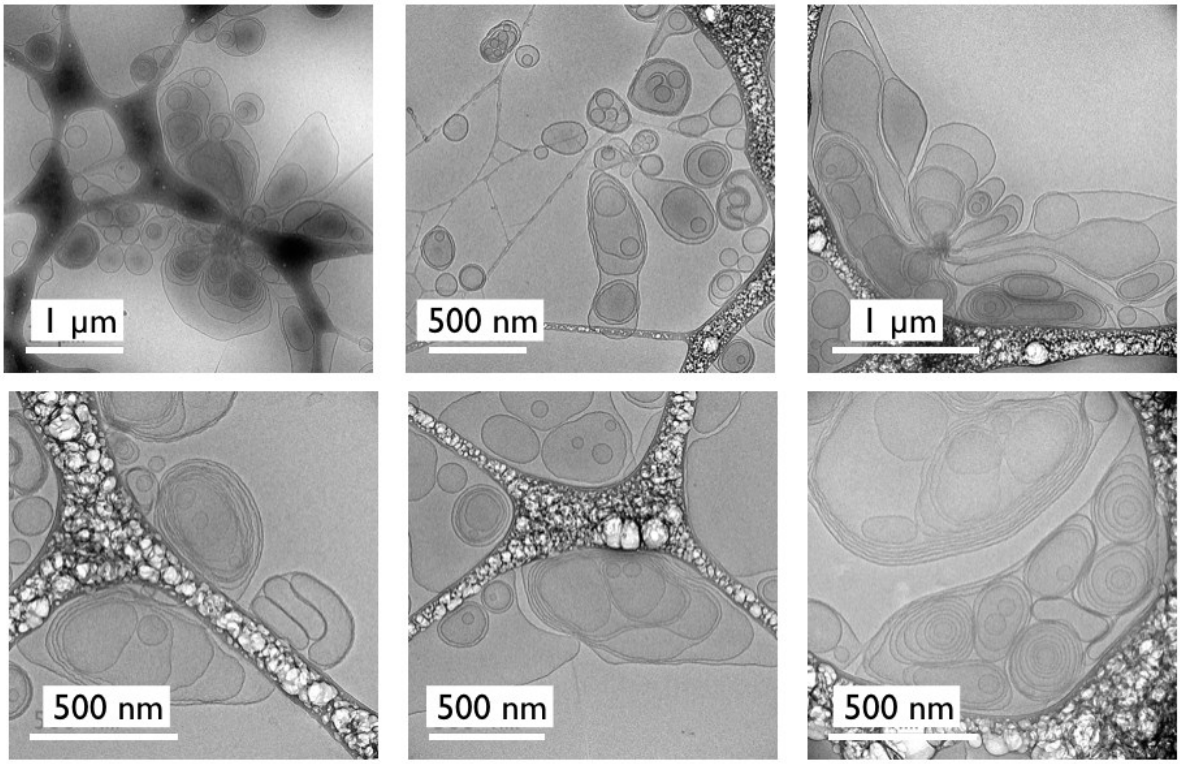

Figure S2: *Cryo-TEM images of Curosurf® vesicles at concentration 5 g L^{-1}.*

Supporting Information S3 – Identity card of the silica particles studied in this work

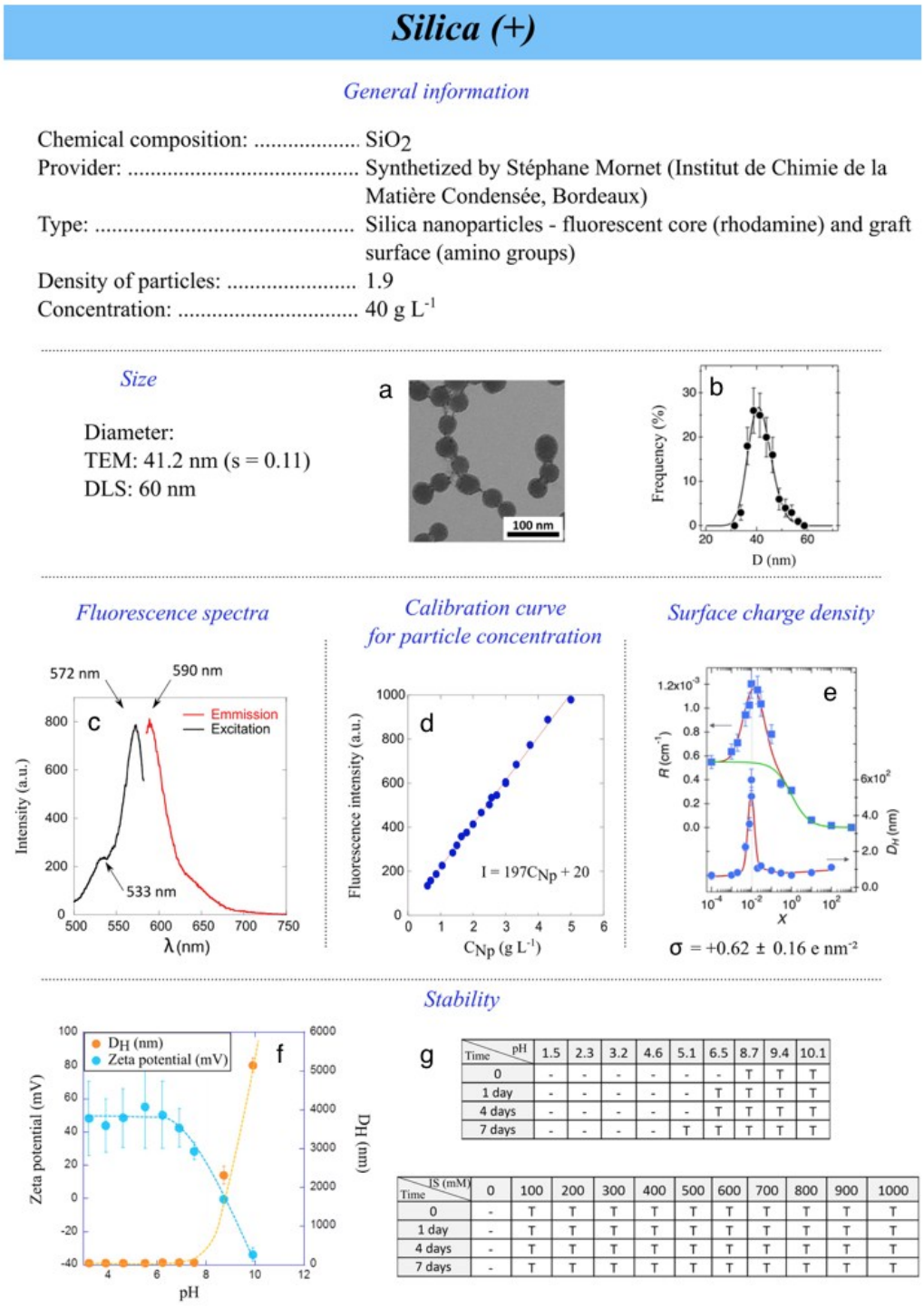

***Figure S3**: Identity card of the silica particles studied in this work.[1] a) TEM image. b) TEM size distribution. c) Excitation and emission fluorescence. d) Calibration curve for particle concentration. e) Surface charge density determined using the Continuous Variation Method with oppositely charged polyelectrolyte.[2] f) Zeta potential and hydrodynamic size as a function of the pH. g) Stability diagram as a function of the ionic strength (NaCl). The letter "T" is for turbid.*

Supporting Information S4 – Calculation of the surface ratio X_S

Nanoparticles

In this section, we derive the available surface developed by the silica nanoparticles. For a dispersion of concentration c_{NP} (g L^{-1}), the number density of particles n_{NP} is given by:

$$n_{NP} = \frac{c_{NP}}{M_n^{NP}} N_A \qquad (S4.1)$$

where M_n is the particle number-average molecular weight and N_A the Avogadro number. n_{NP} is expressed in L^{-1}.

The number-average molecular weight M_n writes:

$$M_n^{NP} = \frac{\pi}{6} \rho D_0^3 exp(4.5 s^2) N_A \qquad (S4.2)$$

For log-normal distribution of median diameter D_0 and dispersity s, the ith-moment is given by the expression $< D^i > = D_0^i exp(i^2 s^2/2)$. In Eq. S4.1, ρ = 1.9 g cm^{-3} is the mass density and N_A the Avogadro number. D_0 = 41.2 nm and s = 0.11 denote the median diameter and the dispersity as determined from TEM.

With the two above equations, we infer the number density of particles noted n_{NP} at a given concentration:

$$n_{NP} = \frac{6 c_{NP}}{\pi \rho D_0^3} exp(4.5 s^2) = 1.36 \times 10^{16} c_{NP} \qquad (S4.3)$$

Assuming that the average surface developed by the particle is $\pi D_0^2 exp(2 s^2)$, the total surface available in the dispersion reads:

$$S_{NP} = \frac{6 c_{NP}}{\rho D_0} exp(-2.5 s^2) = 743600 c_{NP} \qquad (S4.4)$$

where S_{NP} is expressed in cm^2 L^{-1}. According to Eq. S4.4, 1 mL of a silica solution at 1 g L^{-1} corresponds to a nominal surface of 743.6 cm^2.

Vesicles

For molecular calculations, Curosurf® bilayers are assumed to be similar to those made of dipalmitoylphosphatidylcholine (DPPC). For a DPPC dispersion at concentration c (in g L^{-1}), the number density n_{PL} of phospholipids is given by:

$$n_{PL} = \frac{c_{PL}}{M_n^{PL}} N_A \qquad (S4.5)$$

where M_n^{PL} = 734 g mol^{-1}.

The number density of molecules noted n_{PL} at a given concentration, again expressed in L^{-1}:

$$n_{PL} = 8.20 \times 10^{20} c_{PL} \qquad (S4.6)$$

Assuming a surface per polar head of 0.60 nm^2, one gets a total phospholipid surface of:

$$S_{PL} = 8.20 \times 10^{20}\ 60 \times 10^{-16} c_{PL}/2 \qquad (S4.7)$$
$$S_{PL} = 2460000 c_{PL}$$

where S_{PL} is expressed in $cm^2\ L^{-1}$. In Eq. S4.7, the factor 2 arises from the fact that vesicles are made from bilayers and a bilayer cannot coat two different particles. 1 mL of a DPPC dispersion at 1 g L^{-1} corresponds to $S_{PL} = 2460$ cm^2.

For particles and phospholipids mixed at the same concentration, the surface ratio X_S can be expressed as a function of the mixing ratio $X = c_{PL}/c_{NP}$:

$$X_S = \frac{S_{PL}}{S_{NP}} = 3.31X$$

The experiments were performed at X = 0.15, 0.33, 0.39, 0.45, 0.50, 0.59, 1.5 and ∞. The data are displayed in the Table S4 below:

X	X_S	c_{PL} (g L^{-1})	c_{NP} (g L^{-1})
0.15	0.5	0.15	0.85
0.33	1.1	0.28	0.72
0.39	1.3	0.32	0.68
0.45	1.5	0.35	0.65
0.51	1.7	0.34	0.66
0.60	2.0	0.38	0.62
1.51	5	0.60	0.40
∞	∞	1.00	0.00

***Table S4**: Correspondence between the mixing ratio X and the surface ratio X_S. The last two columns show the phospholipid and nanoparticle concentrations, the total concentration being 1 g L^{-1}.*

Supporting Information Figure S5 – Continuous Variation Method for silica nanoparticles and Curosurf® vesicles

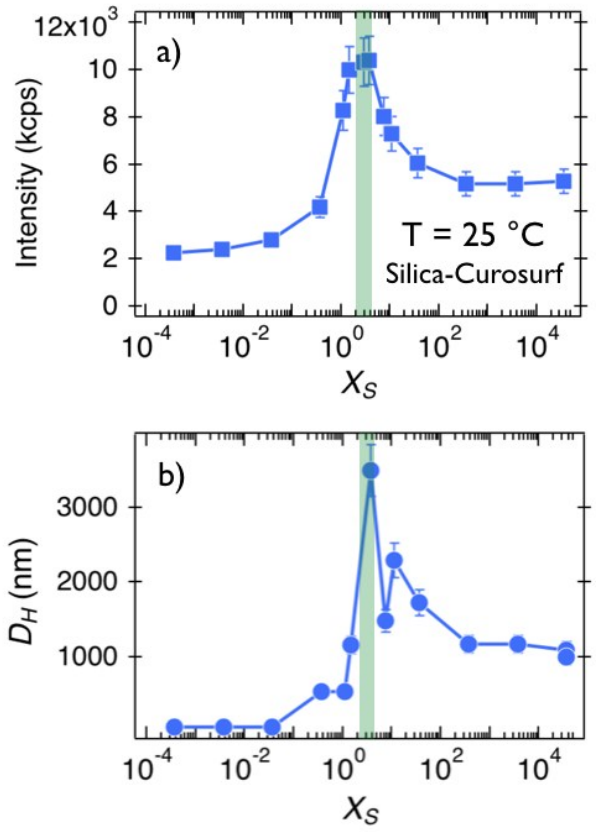

Figure S5: *Scattering intensity (a) and hydrodynamic diameter (b) measured for positively charged 41 nm silica particles complexed with Curosurf® vesicles at concentration* c *= 0.1 g* L^{-1}*. The mixed solutions were prepared at the pH of Curosurf®, i.e. pH 6. The peak position for the intensity and for the diameter coincides and evidences the formation of mixed hybrid vesicle-particle aggregates.*[2-5]

Supporting Information Figure S6 – Liquid-Gel transition from the Curosurf® phospholipid bilayer

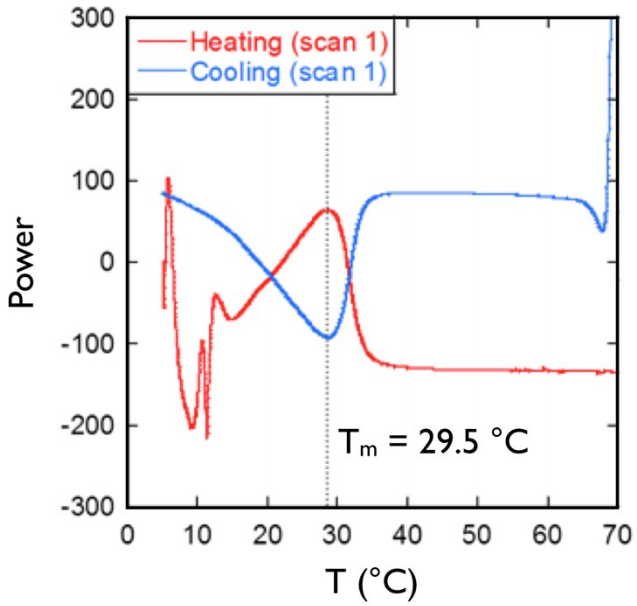

Figure S6: *Thermograms of Curosurf® diluted in DI-water at 10 g L^{-1} obtained by differential scanning calorimetry (DSC). The Curosurf® bilayer melting temperature was estimated at T_m = 29.5 °C from heating and cooling cycles. Thermograms were measured using an N-DSCIII instrument from CSC. The reference cell was filled with Milli-Q water and the sample cell (0.3 mL) with Curosurf®. The capillary cells were not capped and a constant pressure of 5×10^5 Pa was applied. The transition temperature was taken at the second, third and fourth heating scans, at a scan rate of 0.5 °C min^{-1} (from 5 to 70 °C). The melting temperature was estimated as the mean of the three transition temperatures mentioned before. The same procedure was applied with the cooling scans, which were performed in the same conditions.*

Supporting Information S7 – Continuous Variation Method for silica nanoparticles and protein-free surfactant

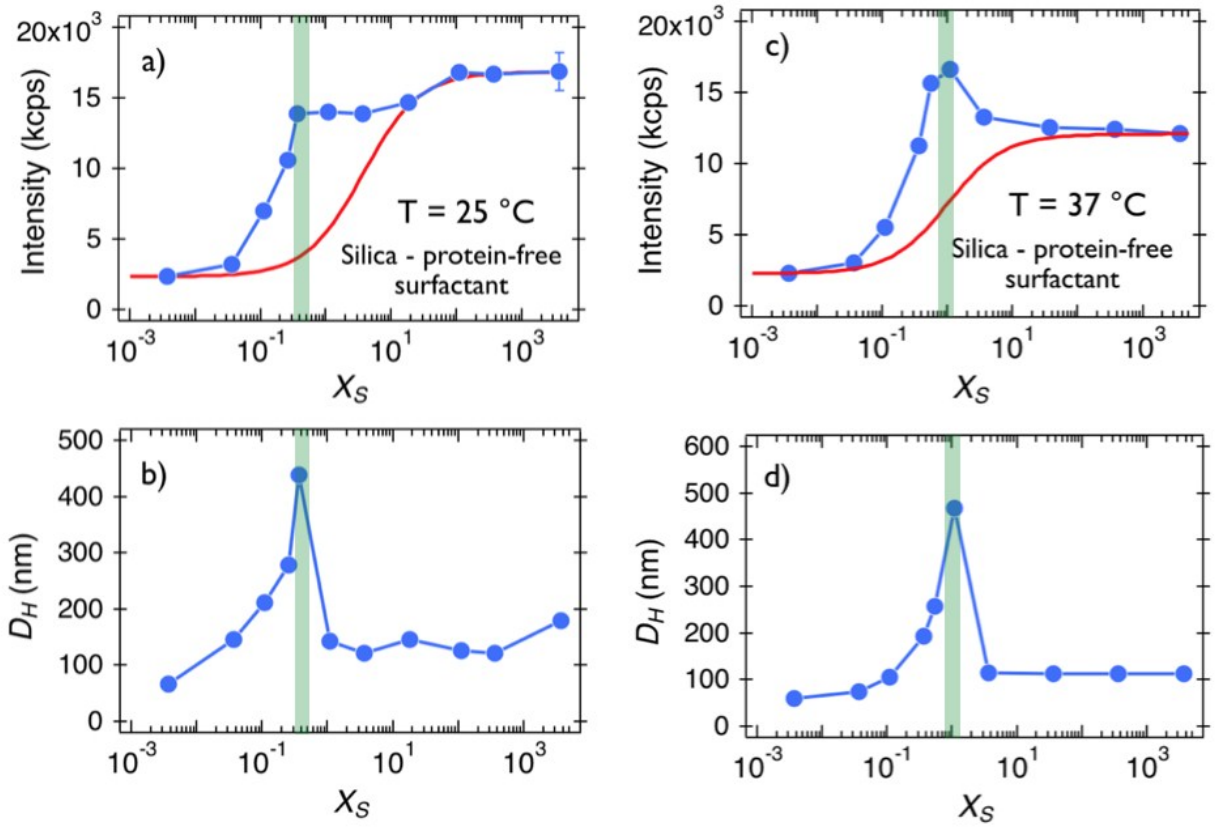

Figure S7: *Results of the Continuous Variation Method applied to a protein-free surfactant and silica particles at 25 and 37 °C.[6] a,c) Scattering intensity and b,d) hydrodynamic diameter as a function of the surface ratio* X_S*. The mixed solutions were prepared at the pH of the Curosurf® (pH 6). For the protein-free surfactant, a mixture of phospholipids was used. Dipalmitoylphospha-tidylcholine (DPPC), L-α-Phosphatidyl-DL-glycerol sodium salt from egg yolk lecithin (PG) and 2-Oleoyl-1-palmitoyl-sn-glycero-3-phospho-rac-(1-glycerol) (POPG) were initially dissolved in methanol, at 10, 10 and 20 g* L^{-1} *respectively. These compounds were mixed in proper amounts for a final weight concentration of 80% / 10% / 10% of DPPC/PG/POPG. The solvent was evaporated under low pressure at 60 °C for 30 minutes. The lipid film formed on the bottom of the flask was then rehydrated with the addition of Milli-Q water at 60 °C and agitated at atmospheric pressure for another 30 minutes. Milli-Q water was added again to finally obtain a solution at 1 g* L^{-1}*.*

Supporting Information S8 – Analysis of Differential Centrifugal Sedimentation data

In Differential Centrifugal Sedimentation (DCS), the particles are injected at the center of the rotation disk containing a sucrose gradient, and sediment according to their sizes. Close to the outer range of the disk, the particles are detected thanks to a laser beam, and the absorbance of the transmitted beam is plotted against the sedimentation time t.

The Stokes relationship allows connecting the sedimentation time t, the particle size D and density ρ according to[7]:

$$(\rho_{NP} - \rho_0) D_{NP}^2 t = cste \qquad (S7.1)$$

where ρ_0 denotes the average sucrose mass density (ρ_0= 1.064 g cm^{-3}). In Eq. S7.1, the constant (*cste*) depends on solution viscosity, centrifuge spin speed, and cell geometry. This constant is determined using a calibration sample of known particle diameter.

For a particle coated with a single supported lipid bilayer, a similar equation holds, namely:

$$(\rho_{nSLB} - \rho_0) D_{nSLB}^2 t = cste \qquad (S7.2)$$

where ρ_{nSLB} and D_{nSLB} are the particle mass density and size, respectively.

The mass density for the coated particles is however unknown, but needs to be entered into the DCS software. For the experiments performed, we thus have a general equation describing the sedimentation kinetics:

$$(\rho_{DCS} - \rho_0) D_{DCS}^2 t = cste \qquad (S7.3)$$

where ρ_{DCS} and D_{DCS} are the mass density and the measured size, respectively. To run the DCS experiments, we thus fixed $\rho_{DCS} = \rho_{NP}$, which leads to a wrong estimation of the sedimentation time-diameter relationship.

To recover the right scaling, a transformation is required. Equating S7.2 and S7.3 leads to:[7]

$$(\rho_{nSLB} - \rho_0) D_{nSLB}^2 = (\rho_{DCS} - \rho_0) D_{DCS}^2 \qquad (S7.4)$$

In addition, the mass density of a coated particle is given by:

$$\rho_{nSLB} = \rho_{SLB} + (\rho - \rho_{SLB}) \frac{D^3}{D_{nSLB}^3} \qquad (S7.5)$$

The combination of the two above relationships leads to a third-degree polynomial:

$$(\rho_0 - \rho_{SLB})D_{nSLB}^3 + (\rho_{DCS} - \rho_0)D_{DCS}^2 D_{nSLB} + (\rho_{SLB} - \rho_{NP})D_{NP}^3 = 0 \qquad (S7.6)$$

Using ρ = 1.9 g cm^{-3} and ρ_{SLB} = 0.9 g cm^{-3},[8,9] D_{NP}= 43.6 nm and D_{DCS} = 40.8 nm (see Table S7 below), one obtains a total diameter D_{nSLB} of 47.2 nm, and a supported lipid bilayer thickness of 1.8 nm. Such a value is lower than the Curosurf® membrane thickness, δ = 4.36 nm, determined from cryo-TEM image analysis.

In conclusion, DCS is an accurate method for determining the particle size and distribution, however in cases of complex colloids a model is generally required to derive more detailed nanostructures. In the present case, DCS underestimates the particle diameter.

	Peak position	
X_S	Absorbance (nm)	Number density (nm)
0	45.0	43.6
1.3	43.4	40.9
1.5	43.7	41.2
1.7	43.5	41.1
2	43.3	40.8
5	43.1	40.9

Table S8: *Positions of the absorbance peaks for bare silica and silica-surfactant dispersions observed by DCS at various coverage ratios X_S. The data are those from Fig. 3. The peak positions of the number distribution are also listed.*

Supporting Information S9 – Additional cryo-TEM images of SLB coated silica nanoparticles

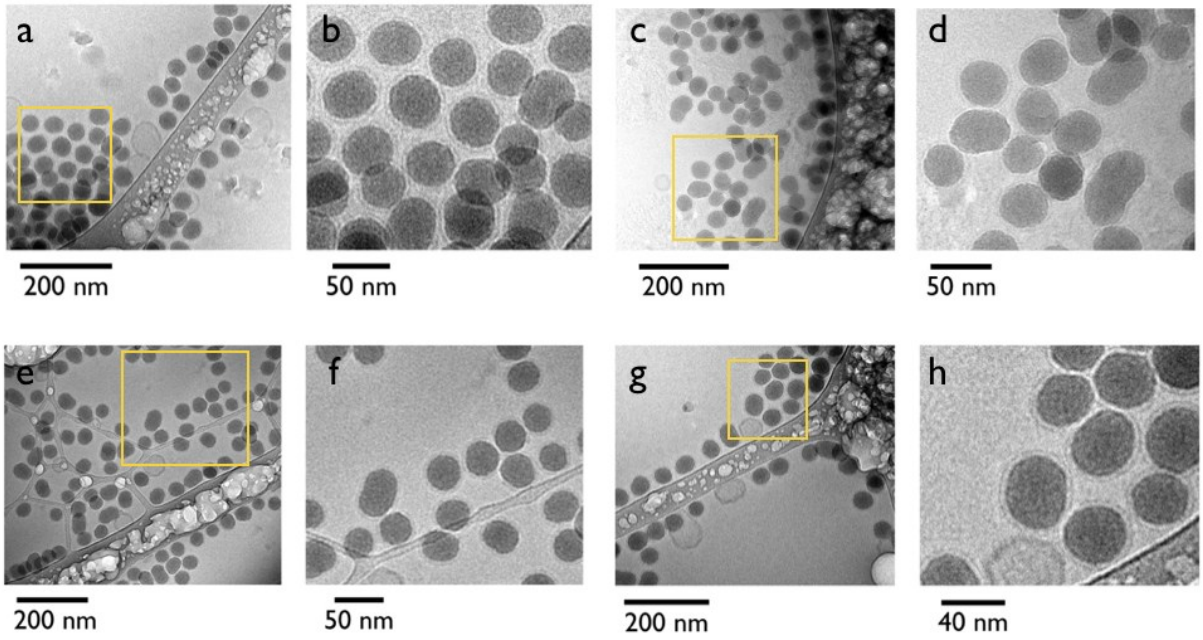

Figure S9: *Additional cryo-TEM images of Curosurf® membrane coated nanoparticles. The experimental conditions were similar to those of Fig. 9.*

Supporting Information Figure S10 – Colloidal stability and zeta potential of SLB coated silica as a function of the time

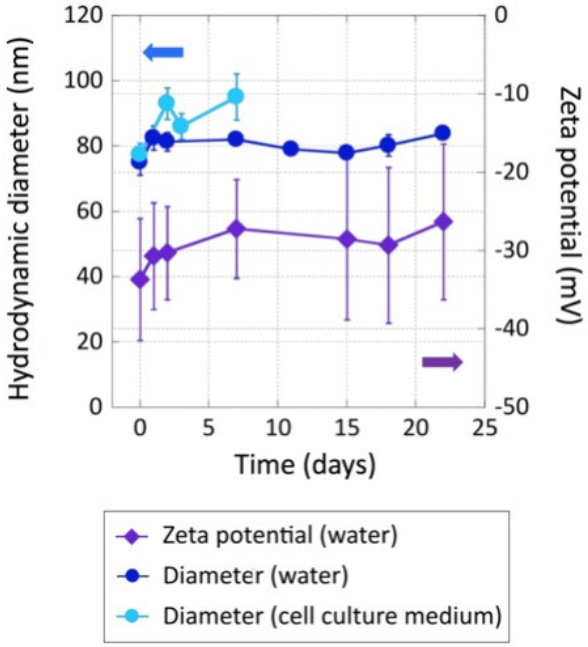

Figure S10: *Colloidal stability and zeta potential of the SLB coated particles as a function of time in different solvents.*

Supporting Information Figure S11 – Continuous Variation Method for SLB coated silica nanoparticles and Curosurf®

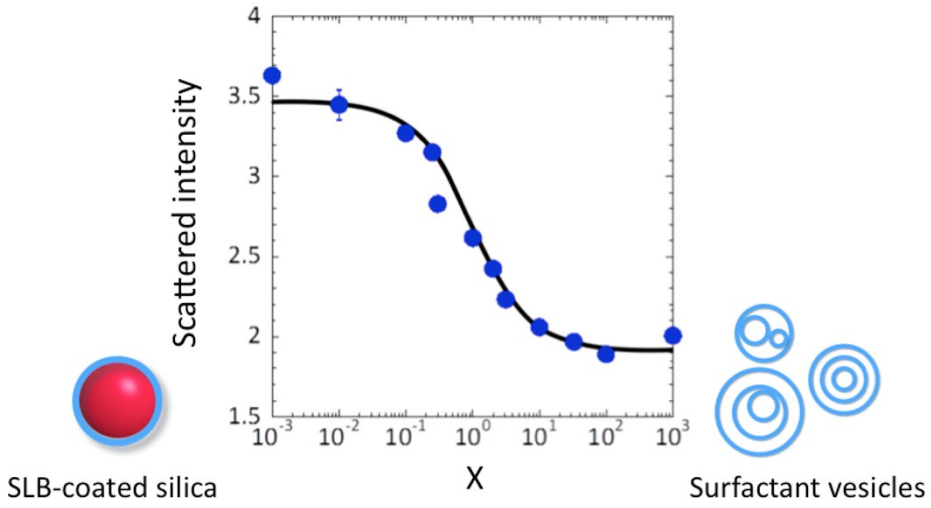

Figure S11: *Results of the Continuous Variation Method applied to SLB coated silica and surfactant vesicles at 25 °C and pH 7.4:[6] The scattering intensity varies continuously from one stock solution (SLB coated silica on the left-hand side) to the other (surfactant vesicles). Here, the intensity is well accounted for by the non-interacting model (continuous line), leading to the conclusion that SLB-coated particles and vesicles do not mutually interact.*

Supporting Information Figure S12 – Confocal microscopy 3D-views of incubated cells

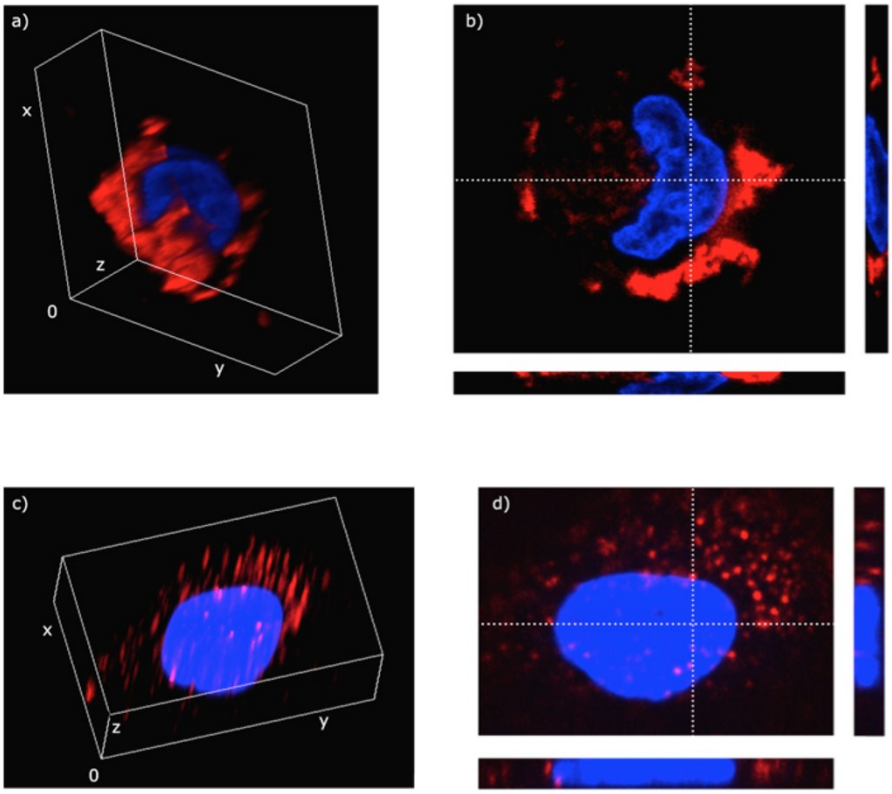

Figure S12: *Confocal images of A549 alveolar epithelial cells incubated with bare silica (a,b) and with silica coated with a supported lipid bilayer (c,d). In a) and d) 3D views of the cells are shown. In b) and d), right and bottom views represent respectively the (x,z)- and (y,z)-slices of the section indicated with the white lines.*

Supporting Information S13 – TEM images of cells incubated with SLB coated silica

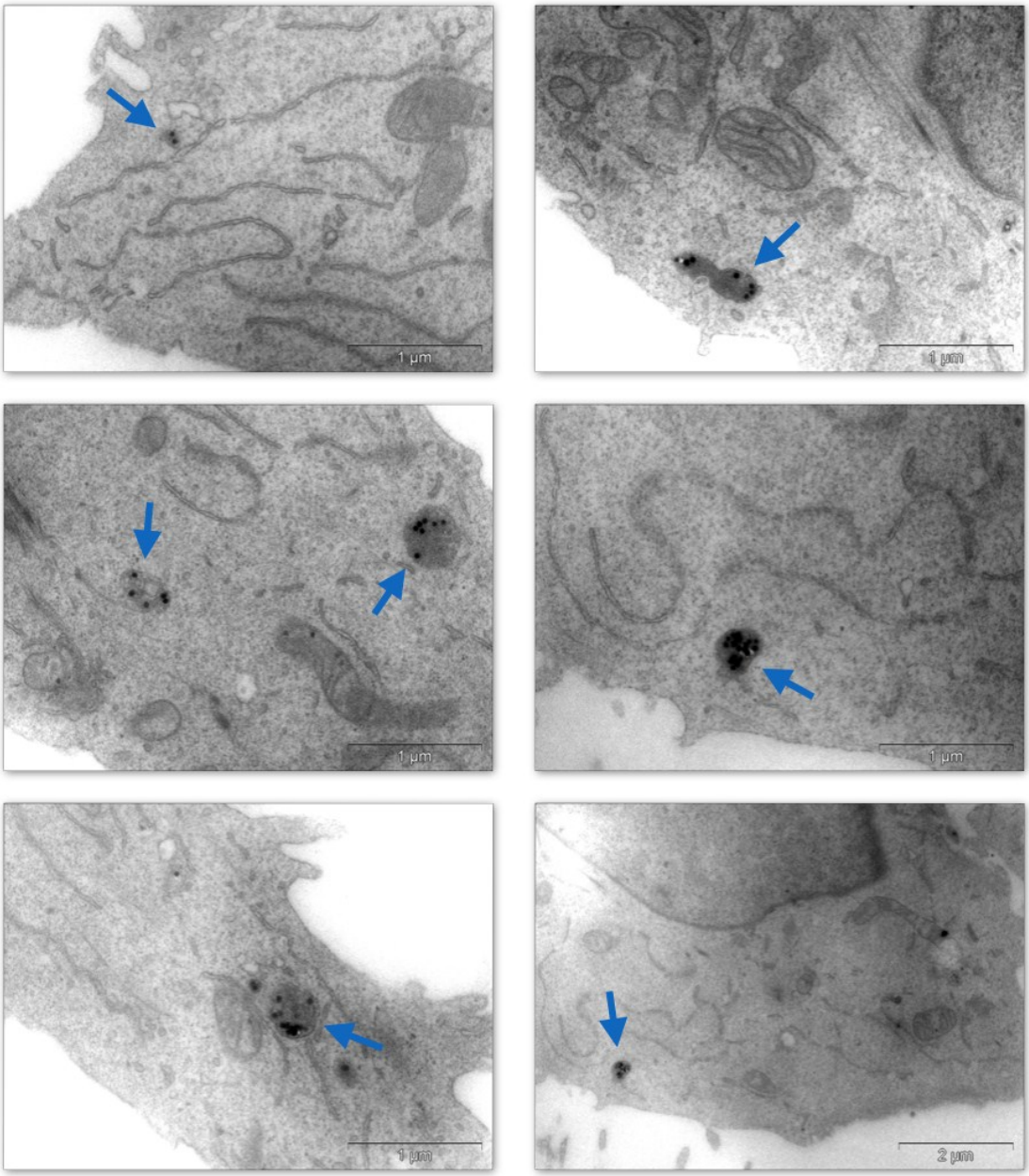

Figure S13: *Additional TEM images of A549 alveolar epithelial cells incubated with SLB-coated silica particles. The arrows are pointing out to nanoparticles enclosed in cellular compartments. The conditions were similar to those of Fig. 9.*

References

1. N. Reinhardt, L. Adumeau, O. Lambert, S. Ravaine and S. Mornet, *J. Phys. Chem. B*, 2015, **119**, 6401-6411.
2. F. Mousseau, L. Vitorazi, L. Herrmann, S. Mornet and J. F. Berret, *J. Colloid Interface Sci.*, 2016, **475**, 36-45.
3. J.-F. Berret, *Macromolecules*, 2007, **40**, 4260-4266.
4. J. Fresnais, C. Lavelle and J.-F. Berret, *J. Phys. Chem. C*, 2009, **113**, 16371-16379.
5. E. K. Oikonomou, F. Mousseau, N. Christov, G. Cristobal, A. Vacher, M. Airiau, C. Bourgaux, L. Heux and J. F. Berret, *J. Phys. Chem. B*, 2017, **121**, 2299-2307.
6. F. Mousseau, R. Le Borgne, E. Seyrek and J.-F. Berret, *Langmuir*, 2015, **31**, 7346-7354.
7. Z. Krpetic, A. M. Davidson, M. Volk, R. Levy, M. Brust and D. L. Cooper, *ACS Nano*, 2013, **7**, 8881-8890.
8. A. A. Gurtovenko and J. Anwar, *J. Phys. Chem. B*, 2009, **113**, 1983-1992.
9. M. Patra, M. Karttunen, M. T. Hyvonen, E. Falck, P. Lindqvist and I. Vattulainen, *Biophys. J.*, 2003, **84**, 3636-3645.